Polymer Testing 85 (2020) 106444

Contents lists available at ScienceDirect

Polymer Testing

journal homepage: http://www.elsevier.com/locate/polytest

Property Modelling

Constitutive modeling of polymers accounting for their hyperelasticity, plasticity, creep and viscoelastic relaxation

Alexander L. Yarin [a,*], Abhilash Sankaran [a], Seongpil An [a,b], Behnam Pourdeyhimi [c]

[a] Department of Mechanical and Industrial Engineering, University of Illinois at Chicago, 842 W. Taylor St., Chicago, IL, 60607-7022, United States
[b] SKKU Advanced Institute of Nanotechnology (SAINT) and Department of Nano Engineering, Sungkyunkwan University (SKKU), Suwon, 16419, Republic of Korea
[c] 3427 The Nonwovens Institute, Box 8301, North Carolina State University, Raleigh, NC, 27695-8301, United States

A B S T R A C T

The hyperelastic Yeoh model has been generalized to account for creep, plasticity and viscoelasticity of polymers. The general tensorial model developed is applied to several rheometric situations: the tensile test used to measure the stress-strain curve in tension, as well as the creep and recovery tests. The resulting equations are compared to the experimental results acquired in the present work for several monolithic synthetic fibers used as specimens. The comparison revealed that the proposed phenomenological rheological constitutive equation is capable of reproducing the experimental data with a uniformly valid set of physical parameters. Moreover, it was possible to accurately predict the residual plastic deformation of the fibers.

1. Introduction

Rubbers and elastomers, in particular, those which are used to form man-made fibers, as well as a number of natural fibers, significantly deviate from the linear elastic response in tensile tests, i.e., demonstrate significant deviations from Hooke's law [1–3]. To describe stress-strain curves in tension observed for such rubber-like and elastomeric materials [4] several phenomenological constitutive equations were proposed, which can be generally characterized as the so-called hyperelastic models [2,5–10]. It should be emphasized that any hyperelastic model is based on a strain energy function W, from which the stress-strain relationships are derived. Some of the commonly used hyperelastic models are the neo-Hookean model, the Mooney-Rivlin model, the Ogden model, the Arruda-Boyce model, and the Yeoh model, etc. [2,5–10]. In many cases fiber-forming materials can be considered being incompressible, and only this type of materials is discussed hereinafter. Several examples of the strain energy function W can be written as

$$W = C_1(I_1 - 3) + C_2(I_2 - 3) \tag{1}$$

where I_1 and I_2 are the first and second invariants of the Green tensor **B**, i.e.

$$I_1 = tr\mathbf{B}, \quad I_2 = tr\mathbf{B}^2 \tag{2}$$

and C_1 and C_2 are the material parameters.

Then, the stress tensor **σ** is found from the strain energy function, for example as

$$\boldsymbol{\sigma} = -\frac{2}{3}\left(I_1\frac{\partial W}{\partial I_1} + 2I_2\frac{\partial W}{\partial I_2}\right)\mathbf{I} + 2\left[\left(\frac{\partial W}{\partial I_1} + I_1\frac{\partial W}{\partial I_2}\right)\mathbf{B} - \frac{\partial W}{\partial I_2}\mathbf{B}\cdot\mathbf{B}\right] \tag{3}$$

where **I** is the unit tensor.

Substituting Eq. (1) into Eq. (3), one arrives at the following equation

$$\boldsymbol{\sigma} = -\frac{2}{3}(C_1I_1 + 2C_2I_2)\mathbf{I} + 2[(C_1 + C_2I_1)\mathbf{B} - C_2\mathbf{B}\cdot\mathbf{B}] \tag{4}$$

The latter can be transformed into the incompressible Mooney-Rivlin constitutive model

$$\boldsymbol{\sigma} = -p\mathbf{I} + 2C_1\mathbf{B} - 2C_2\mathbf{B}^{-1} \tag{5}$$

where the isotropic part $(-2C_1I_1 + 2C_2I_2)/3$ is absorbed into pressure. Note that the limiting case of Hooke's law, which should be inevitably recovered at small strains, requires that $2(C_1 + C_2) = G$, with G being the shear modulus.

Such, and more complex hyperelastic models can successfully describe the stress-strain curves of several elastomeric fibers with a proper choice of the material constants C_1, C_2, etc. However, these models are based on a potential energy, and thus imply that the unloading will proceed along the same curve in the opposite direction, and any strain will vanish. This contradicts to the fact that polymers which were stretched to significant (finite) strains reveal a non-zero

* Corresponding author.
E-mail address: ayarin@uic.edu (A.L. Yarin).

https://doi.org/10.1016/j.polymertesting.2020.106444
Received 29 November 2019; Received in revised form 14 February 2020; Accepted 15 February 2020
Available online 18 February 2020

residual strain after unloading (as demonstrated, in particular, in the present work), and thus, possess an irreversible plastic deformation [11,12]. Accordingly, the shape of the nonlinear stress-strain curves of elastomers is inevitably affected by plasticity, hence if strains are large enough hence, the hyperelastic models should be generalized to account for the plastic behavior.

Experimental studies conducted with different polymers revealed rheological behavior which manifests non-linear elasticity, and almost ideal plasticity, or plasticity with strain hardening, strain-rate effects, creep and viscoelastic relaxation effects [13–17], as well as temperature-dependent deformation [18,19]. Relaxation and fatigue of polymers were probed using the cyclic-load test [20,21], which also revealed the history-dependent characteristics of polymers in addition to the intrinsic damage associated with plasticity.

Viscoelasticity of polymer fibers had attracted considerable attention [3,22]. A comprehensive discussion of different relaxation processes in polymers and their molecular origin can be found in Ref. [22]. The techniques used to probe the molecular relaxation mechanisms involve the indirect integral mechanical and dielectric responses, as well as such molecular responses as the nuclear magnetic resonance and scattering techniques. In addition, molecular dynamics simulation are employed to understand the molecular motions responsible for the relaxation mechanisms [22].

Rheological constitutive equations of polymers involve phenomenological or micromechanical approaches, where the former is based on the macroscopic observations, whereas the latter – on detailed material models. The micromechanical modeling is facilitated by atomistic simulations [23,24], which is a bottom-up, computationally-intensive approach.

Phenomenological models which account for viscoplasticity/dissipation of polymer fibers were also reported [25,26] and strain-rate effects were accounted for [25]. However, a non-linear increase in stress at high strains observed for some polymers (like in Ref. [7] for rubber, or in the present work), as well as creep cannot be described by them. An overstress model intended to capture creep, plasticity and strain-rate effect was proposed in Ref. [27] where the viscosity coefficient (related to the relaxation time) is taken as a non-linear function of stress. However, the latter model is not presented in the invariant tensorial form and also cannot be generalized for hyperelastic behavior.

A model based on network alteration theory used to describe the fatigue characteristics of styrene-butadiene rubber was developed in Ref. [28]. The model utilizes the Arruda and Boyce hyperelastic strain energy density for the network stress-strain relation and viscous behavior, which arises due to molecular relaxation because of the molecular chain reptations. A further development of a similar approach incorporated the recoverable viscoelasticity and the effect of thermal dissipation on fatigue of rubbers, [29]. A viscoelastic – hyperelastic model was developed in Ref. [30] based on a strain-energy function with two exponential terms depending on the tensor invariants. The model of [30] successfully predicted the characteristic times of force rise for the applied torsional and radial displacement ramp tests in addition to the stress-strain relations for the deformation modes. However, the model of [30] did not incorporate plastic deformation.

The works where the rheological constitutive models incorporate simultaneously the non-linear elasticity, plasticity, creep and viscoelastic relaxation are scarce. Cyclic creep - recovery and cyclic tensile-tensile behavior of polymer composites were described by the phenomenological model accounting for their viscoelastic and viscoplastic characteristics in Ref. [20]. A viscoelastic – viscoplastic constitutive model for asphalt material was proposed in Ref. [31] accounting for creep under tension and compression for different temperatures. The model involves multiple material parameters even at the reference temperature.

The attempts to understand rheological behavior of semi-crystalline polymers based on the microscale crystalline and amorphous models were undertaken in Refs. [32–34]. In the framework of the micromechanical approach, Refs. [35,36], the hyperelastic and viscoplastic behavior of semi-crystalline polymers was accounted for. However, this approach inevitably involves multiple physical parameters, whose values are unknown at present. A general invariant tensorial constitutive phenomenological model of polymers should be inevitably linked to macromolecular chain stretching and their interaction with each other [37].

Mechanical behavior of polymers determined by their rheological constitutive equations is important not only for monolithic materials, but also for polymer composites [24,38] and nonwovens [39,40].

In the present work, a general invariant tensorial model which accounts for hyperelasticity, plasticity, creep and viscoelasticity of polymers is attempted and compared to the experimental data for many polymers. Simple rheological constitutive relations, which incorporate linear elastic response, creep and the viscoelastic memory effects can be reduced to the equations discussed next. Creep and viscoelasticity in one-dimensional situation are described as [12]

$$\varepsilon(t)=\frac{1}{E}\left[\sigma(t)+(\gamma-\mu)\int_{-\infty}^{t}\sigma(\tau)e^{-\mu(t-\tau)}d\tau\right] \tag{6}$$

where ε is the strain, σ is the stress, t is time, τ is the dummy variable, E = 3G is Young's modulus, and γ and μ are the inverse stress relaxation time, and the inverse strain retardation time, respectively. It should be emphasized that γ>μ.

Equation (6) can be transformed to the form resolved for the stress

$$\sigma(t)=E\left[\varepsilon-(\gamma-\mu)\int_{-\infty}^{t}\varepsilon(\tau)e^{-\gamma(t-\tau)}d\tau\right] \tag{7}$$

Note, that both integral equations (6) and (7) are identical to the following differential equation

$$\frac{d\sigma}{dt}+\gamma\sigma=E\left(\frac{d\varepsilon}{dt}+\mu\varepsilon\right) \tag{8}$$

where d/dt denotes the material time derivative. Note also that Eqs. (6)–(8) imply the exponentially fading memories for stress relaxation and strain retardation.

For tensile tests conducted at a constant strain rate $\dot{\varepsilon}$, the strain is equal to $\varepsilon(t)=\dot{\varepsilon}t$. Substituting the latter into Eq. (7), one obtains the following stress-strain dependence

$$\sigma=E\left[\frac{\mu}{\gamma}\varepsilon+\frac{\dot{\varepsilon}}{\gamma}\left(\frac{-\mu}{\gamma}+1\right)-\frac{(\gamma-\mu)\dot{\varepsilon}}{\gamma^2}\exp\left(-\frac{\gamma\varepsilon}{\dot{\varepsilon}}\right)\right] \tag{9}$$

At time t = 0, ε is equal to zero, and accordingly Eq. (9) yields σ = 0.

Initially at very small strains, i.e., at $\varepsilon\to0$, the result obtained from Eq. (9) reveals the linear dependence of stress on strain, which is in accordance with Hooke's law, namely

$$\sigma=E\varepsilon \tag{10}$$

As the strain increases, Eq. (9) reveals a non-linear behavior, which is due to the exponential term present in the equation, which has nothing in common with hyperelasticity or plasticity. It also reveals the dependence of the stress-strain curve on strain rate $\dot{\varepsilon}$. At very large strain, i.e., at $\varepsilon\to\infty$, Eq. (9) reveals a linear behavior once again, albeit different from that of Eq. (10). Namely, the second linear asymptote takes the form

$$\sigma=E\left(\frac{\mu}{\gamma}\right)\varepsilon \tag{11}$$

This dependence is weaker than that of Eq. (10), since the ratio $\mu/\gamma<1$. The overall behavior of Eq. (9) is sketched in Fig. 1.

Creep and viscoelastic relaxation predicted by Eq. (6) are illustrated by the following situation. Let a fiber be fully unloaded at t = 0, i.e. at t = 0, the stress σ = 0. Let at t = +0 the fiber is stretched instantaneously

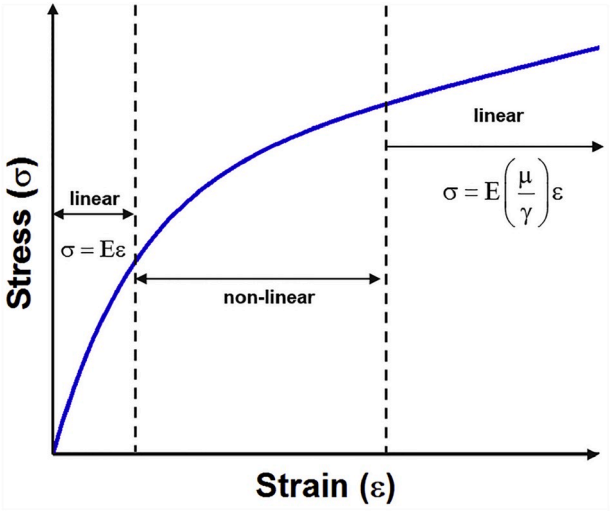

Fig. 1. The overall stress-strain curve in tensile test predicted by Eq. (9).

with a constant stress σ_0 and then during the time interval $0 < t \le t_1$ is held at this stress. Then, Eq. (6) yields for this time period the following dependence of strain on time

$$\varepsilon(t) = \frac{\sigma_0}{E}\left[1 + \frac{\gamma - \mu}{\mu}(1 - e^{-\mu t})\right] \quad at \quad 0 < t \le t_1 \tag{12}$$

The latter shows that there is an immediate elastic response

$$\varepsilon_{\text{elastic}} = \frac{\sigma_0}{E} \tag{13}$$

corresponding to Hooke's law, followed by a time-dependent creep under load

$$\varepsilon_{creep}(t) = \frac{\sigma_0}{E}\frac{(\gamma - \mu)}{\mu}(1 - e^{-\mu t}) \quad at \quad 0 < t \le t_1 \tag{14}$$

The maximum creep achieved at $t = t_1$ is

$$\varepsilon(t_1) = \varepsilon_{\max} = \frac{\sigma_0}{E}\left[1 + \frac{\gamma - \mu}{\mu}(1 - e^{-\mu t_1})\right] \tag{15}$$

Then, let the fiber loading ceases at $t = t_1$, i.e., at $t > t_1$, the stress $\sigma = 0$. Then, Eq. (6) yields

$$\varepsilon(t) = \frac{(\gamma - \mu)}{\mu}\frac{\sigma_0}{E}[e^{-\mu(t - t_1)} - e^{-\mu t}] \quad at \quad t_1 < t < \infty \tag{16}$$

It is instructive to see that Eq. (16) predicts a different value of $\varepsilon(t_1)$ than Eq. (15), namely

$$\varepsilon(t_1) = \frac{(\gamma - \mu)}{\mu}\frac{\sigma_0}{E}[1 - e^{-\mu t_1}] \tag{17}$$

Specifically, the value predicted by Eq. (15) is by σ_0/E higher than the one predicted by Eq. (17). This means that an immediate elastic shrinkage happens at the unloading moment. Then, the rest of the strain relaxes to zero, i.e., $\varepsilon \to 0$, as $t \to \infty$, because Eqs. (6)–(8) do not incorporate plasticity. The strain history described by Eqs. (14) and (16) is depicted in Fig. 2.

The general tensorial nonlinear elastic-plastic constitutive models, which do not incorporate creep and viscoelastic relaxation of the type of models (6)–(8) were introduced in Refs. [41–44]. These general tensorial models are presented in the form of a differential equation, which makes them convenient and accurate in description of transient deformation processes. The variant of interest in the present work which was already used in situations with uniaxial elongation in Ref. [45] reads

$$\boldsymbol{\sigma} = -p\mathbf{I} + \boldsymbol{\tau} \tag{18}$$

$$\boldsymbol{\tau} = \mathbf{F}\cdot\mathbf{S}\cdot\mathbf{F}^T \tag{19}$$

$$\mathbf{S} = -G\left(\mathbf{C}^{-1}\cdot\mathbf{C}_p\cdot\mathbf{C}^{-1} - \frac{\mathbf{C}_p : \mathbf{C}^{-1}}{3}\mathbf{C}^{-1}\right) \tag{20}$$

$$\frac{d\mathbf{C}_p}{dt} = \Gamma\left(\frac{3}{\mathbf{C}_p^{-1} : \mathbf{C}}\mathbf{C} - \mathbf{C}_p\right) \tag{21}$$

where $\boldsymbol{\tau}$ is the deviatoric stress tensor, $\mathbf{F}$ is the gradient of deformation tensor, $\mathbf{C} = \mathbf{F}^T\cdot\mathbf{F}$ is the Cauchy tensor, $\mathbf{S}$ is the deviator of the Piola-Kirchhoff tensor, $\mathbf{C}_p$ is the plastic deformation tensor, Γ is the plasticity parameter. The latter is given by the following expression

$$\Gamma = \Gamma_0 \exp\left[-\frac{1}{2}\left(\frac{Z}{\sigma_c}\right)^{2n}\right] \tag{22}$$

with Γ_0, Z and n being the material parameters, and σ_c being the von Mises stress, $\sigma_c = (\boldsymbol{\sigma} : \boldsymbol{\sigma})^{1/2}$.

The aim of the present work is to develop a modified constitutive model and test it experimentally using such specimens as polymer fibers in tensile tests up to large strains, as well as in the creep and recovery experiments. The results are expected to reveal non-linear hyperelasticity, plasticity, creep and viscoelastic relaxation.

2. Experimental

In the experiments different synthetic monofilament fibers were used as the specimens. The tests were conducted using the Dynamic Mechanical Analysis (DMA) machine (model Q 800). The room temperature during the tests was ~22 °C and the relative humidity (RH) is

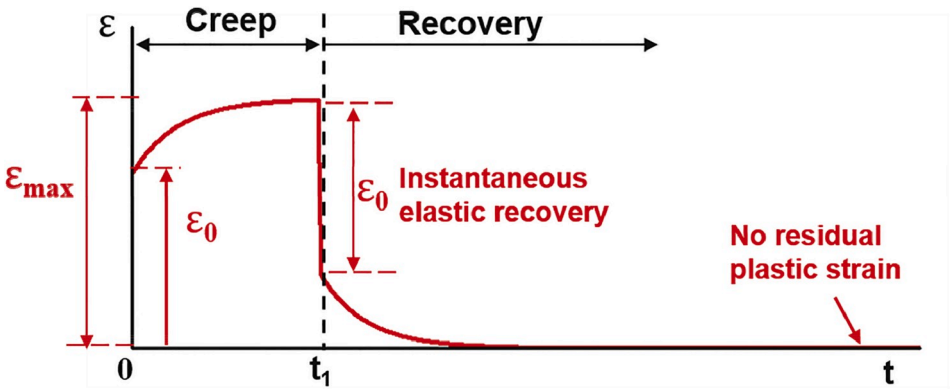

Fig. 2. Creep and viscoelastic relaxation according to the model (6).

mentioned for each fiber type. The average diameters of the fibers used in the experiments are listed in Table 1.

Tensile tests of the fibers were conducted at a constant stretching rate. Three trials were performed for each condition. For each trial, a new specimen was used. The initial length of each specimen was approximately 10 mm except for polypropylene. For polypropylene fiber initial length of approximately 6.5 mm was utilized which was determined by their small diameters.

Creep and recovery tests were conducted under tension, with a new specimen each run. The creep experiments were conducted under stresses of 20, 40, 80, 120 and 160 MPa. The duration of the creep and recovery stages was 10 min and 100 min, respectively, for all the experiments.

3. Phenomenological constitutive equation accounting for hyperelasticity, plasticity, creep and viscoelastic relaxation

3.1. Rheological constitutive equation

As a starting point, we chose the hyperelastic model of Ref. [7]. This is related to the fact that if simpler neo-Hookean or Mooney-Rivlin sub-models [2] would be generalized to include plasticity and viscoelasticity, they still could not capture the non-linear increase in stress at higher stresses (corresponding to the so-called strain hardening) characteristic of many polymers (cf. section 4). Additionally, one can simplify the Yeoh model to neo-Hookean or Mooney Rivlin by choosing appropriate constants.

The nonlinear strain energy function considered in Ref. [7] is in the form

$$W = C_1(I_1-3) + C_2(I_1-3)^2 + C_3(I_1-3)^3 \tag{23}$$

where $I_1 = tr\mathbf{B}$, and C_1, C_2 and C_3 are the physical constants.

Then, the traceless deviatoric stress tensor of the Yeoh model takes the form [7]

$$\boldsymbol{\tau} = 2\left[C_1 + 2C_2(I_1-3) + 3C_3(I_1-3)^2\right]\left[\mathbf{B} - (\mathbf{B}:\mathbf{I})\frac{\mathbf{I}}{3}\right] \tag{24}$$

where the Green tensor $\mathbf{B} = \mathbf{F}.\mathbf{F}^{\mathrm{T}}$.

In the spirit of the modification of the neo-Hookean hyperelastic model in [41–44], Eq. (24) is modified as follows to account for plasticity

$$\boldsymbol{\tau} = 2\left[C_1 + 2C_2(I_1-3) + 3C_3(I_1-3)^2\right]\left\{\mathbf{F}\cdot\mathbf{C}_p^{-1}\cdot\mathbf{F}^T - \left[\left(\mathbf{F}\cdot\mathbf{C}_p^{-1}\cdot\mathbf{F}^T\right) : \mathbf{I}\right]\frac{\mathbf{I}}{3}\right\} \tag{25}$$

where the plastic deformation tensor $\mathbf{C}_\mathrm{p}$ is given by Eq. (21).

Consider an axially-symmetric incompressible fiber-like specimen which undergoes uniaxial deformation. Then, the gradient of deformation tensor $\mathbf{F}$ corresponds to the following matrix

$$(\mathbf{F}) = \begin{pmatrix} \lambda & 0 & 0 \\ 0 & \lambda^{-1/2} & 0 \\ 0 & 0 & \lambda^{-1/2} \end{pmatrix} \tag{26}$$

Table 1
Different fibers tested and their diameter.

Fiber	Diameter (μm)
Nylon 6,6	150
Polyethylene terephthalate (PET)	200
Polybutylene terephthalate (PBT)	180
Polypropylene (PP)	44
Polytetrafluoroethylene (PTFE)	635
Polyethyletherketone (PEEK)	150

with λ being the stretching ratio in the axial direction.

Accordingly, the Green tensor corresponds to the following matrix

$$(\mathbf{B}) = \begin{pmatrix} \lambda^2 & 0 & 0 \\ 0 & \lambda^{-1} & 0 \\ 0 & 0 & \lambda^{-1} \end{pmatrix} \tag{27}$$

and the plastic deformation tensor corresponds to

$$(\mathbf{C}_p) = \begin{pmatrix} \lambda_p^2 & 0 & 0 \\ 0 & \lambda_p^{-1} & 0 \\ 0 & 0 & \lambda_p^{-1} \end{pmatrix} \tag{28}$$

In Eq. (28) λ_p denotes the plastic stretching ratio.

Substituting Eqs. (26)–(28) into Eq. (25), one finds the deviatoric stresses in the following form

$$\tau_{xx} = 2\left[C_1 + 2C_2(I_1-3) + 3C_3(I_1-3)^2\right]\left[\frac{2}{3}\left(\frac{\lambda^2}{\lambda_p^2} - \frac{\lambda_p}{\lambda}\right)\right] \tag{29}$$

$$\tau_{yy} = \tau_{zz} = 2\left[C_1 + 2C_2(I_1-3) + 3C_3(I_1-3)^2\right]\left[\frac{1}{3}\left(\frac{\lambda_p}{\lambda} - \frac{\lambda^2}{\lambda_p^2}\right)\right] \tag{30}$$

where the x-axis corresponds to the fiber axis, and the y- and z-axes are the two additional Cartesian axes in the fiber cross-section; also, $I_1 = tr\mathbf{B} = \lambda^2 + 2/\lambda$.

According to Eq. (18), the corresponding stresses are given by the following expressions

$$\sigma_{xx} = -p + \tau_{xx}, \quad \sigma_{yy} = \sigma_{zz} = -p + \tau_{yy} \tag{31}$$

Because the lateral surface of the fiber is traction- and load-free, $\sigma_{yy} = \sigma_{zz} = 0$ everywhere, and the second Eq. (31) yields the pressure as $p = \tau_{yy}$. Substituting the latter into the first Eq. (31), one obtains $\sigma_{xx} = \tau_{xx} - \tau_{yy}$. Then, using Eqs. (29) and (30), one finds

$$\sigma_{xx} = 2\left[C_1 + 2C_2(I_1-3) + 3C_3(I_1-3)^2\right]\left(\frac{\lambda^2}{\lambda_p^2} - \frac{\lambda_p}{\lambda}\right) \tag{32}$$

In the limit of small strains $\varepsilon \to 0$ the response is purely elastic, i.e. $\lambda_p \equiv 1$, and $\lambda \to 1 + \varepsilon$. Then, Eq. (32) yields

$$\sigma_{xx} = 6C_1\varepsilon \tag{33}$$

which is nothing but Hooke's law, where the constant $C_1 = G/2 = E/6$, as expected. On the other hand, the constants C_2 and C_3 can be determined only in the non-linear regimes corresponding to higher strains.

Equation (32) may be rewritten as

$$\sigma_{xx} = GK(\lambda)\left(\frac{\lambda^2}{\lambda_p^2} - \frac{\lambda_p}{\lambda}\right) \tag{34}$$

where, $K(\lambda) = \{1 + 4C_2'[I_1(\lambda) - 3] + 6C_3'[I_1(\lambda) - 3]^2\}$, with $I_1(\lambda) = \lambda^2 + 2/\lambda$, $C_2' = C_2/G$ and $C_3' = C_3/G$.

In addition, substituting Eqs. (26)–(28) into Eqs. (21) and (22), one obtains the differential equation describing the plastic deformation

$$\frac{d\lambda_p}{dt} = \Gamma\frac{\lambda_p\left(\lambda^3 - \lambda_p^3\right)}{\left(\lambda^3 + 2\lambda_p^3\right)}, \quad \Gamma = \Gamma_0\exp\left[-\frac{1}{2}\left(\frac{Z}{\sigma_{xx}}\right)^{2n}\right] \tag{35}$$

which is solved in stretching with the following initial condition

$$t = 0, \quad \lambda_p = 1 \tag{36}$$

Note that during unloading (recovery), plastic deformation is 'frozen' at its largest value achieved during loading [11], and thus, $d\lambda_p/dt = 0$ during unloading.

It should be emphasized that Eq. (34) shows that the measure of the nonlinear elastic-plastic deformation is $K(\lambda)(\lambda^2/\lambda_p^2 - \lambda_p/\lambda)$. Accordingly, Eqs. (6)–(8) can be generalized to the following three identical constitutive equations which incorporate the nonlinear elasticity (hyperelasticity), plasticity, creep, and viscoelastic relaxation

$$K(t)\left[\frac{\lambda^2(t)}{\lambda_p^2(t)}-\frac{\lambda_p(t)}{\lambda(t)}\right]=\frac{1}{G}\left[\sigma_{xx}(t)+(\gamma-\mu)\int_{-\infty}^{t}\sigma_{xx}(\tau)e^{-\mu(t-\tau)}d\tau\right] \tag{37}$$

$$\sigma_{xx}(t)=G\left\{K(t)\left[\frac{\lambda^2(t)}{\lambda_p^2(t)}-\frac{\lambda_p(t)}{\lambda(t)}\right]-(\gamma-\mu)\int_{-\infty}^{t}\left[\frac{\lambda^2(\tau)}{\lambda_p^2(\tau)}-\frac{\lambda_p(\tau)}{\lambda(\tau)}\right]K(t)e^{-\gamma(t-\tau)}d\tau\right\} \tag{38}$$

$$K(t)\frac{d}{dt}\left[\frac{\lambda^2(t)}{\lambda_p^2(t)}-\frac{\lambda_p(t)}{\lambda(t)}\right]+\mu K(t)\left[\frac{\lambda^2(t)}{\lambda_p^2(t)}-\frac{\lambda_p(t)}{\lambda(t)}\right]=\frac{1}{G}\left[\frac{d\sigma_{xx}(t)}{dt}+\gamma\sigma_{xx}(t)\right] \tag{39}$$

where $K(t) = K[\lambda(t)]$.

Each of these equations is supplemented with Eq. (35) with the initial condition (36).

3.2. Constitutive equation applied to tensile test

Consider fiber stretching with a constant rate of strain $\dot{\varepsilon}$. Then, the strain increases as $\varepsilon = \dot{\varepsilon}t$, and thus, $\lambda = \exp(\dot{\varepsilon}t) = \exp(\varepsilon)$. Then, Eq. (38) yields

$$\sigma_{xx}(t)=G\left\{K(t)\left[\frac{e^{2\varepsilon(t)}}{\lambda_p^2(t)}-\frac{\lambda_p(t)}{e^{\varepsilon(t)}}\right]-(\gamma-\mu)\int_{-\infty}^{t}\left[\frac{e^{2\dot{\varepsilon}\tau}}{\lambda_p^2(\tau)}-\frac{\lambda_p(\tau)}{e^{\dot{\varepsilon}\tau}}\right]K(t)e^{-\lambda(t-\tau)}d\tau\right\} \tag{40}$$

where

$$K(t)=\left[1+4C_2'\left(\frac{e^{2\dot{\varepsilon}t}}{\lambda_p^2}+2\frac{\lambda_p}{e^{\dot{\varepsilon}t}}-3\right)+6C_3'\left(\frac{e^{2\dot{\varepsilon}t}}{\lambda_p^2}+2\frac{\lambda_p}{e^{\dot{\varepsilon}t}}-3\right)^2\right] \tag{41}$$

Accordingly, the stress-strain dependence is found from Eq. (40), together with Eq. (35) integrated numerically using the Kutta-Merson method subjected to the initial condition (36). The resulting stress-strain curve is shown in Fig. 3, and the corresponding dependences for the plastic stretching ratio λ_p and the ratio λ_p/λ on ε – in Figs. 4 and 5,

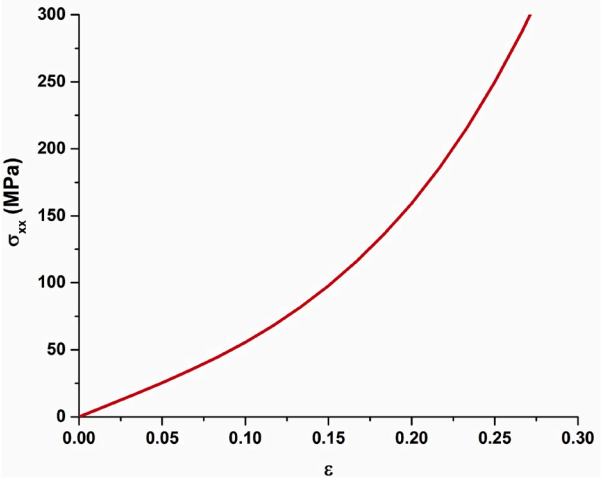

Fig. 3. Nonlinear elastic-plastic stress-strain curve accounting for creep and viscoelastic relaxation predicted by Eqs. (35), (36) and (38) with the following values of the parameters: $\dot{\varepsilon} = 0.001\ s^{-1}$, $\gamma = 0.006\ s^{-1}$, $\mu = 0.004\ s^{-1}$, E = 500 MPa, $C_2 = 200$ MPa, $C_3 = 10$ MPa, $\Gamma_0 = 0.0003\ s^{-1}$, Z = 20 MPa, and n = 1.

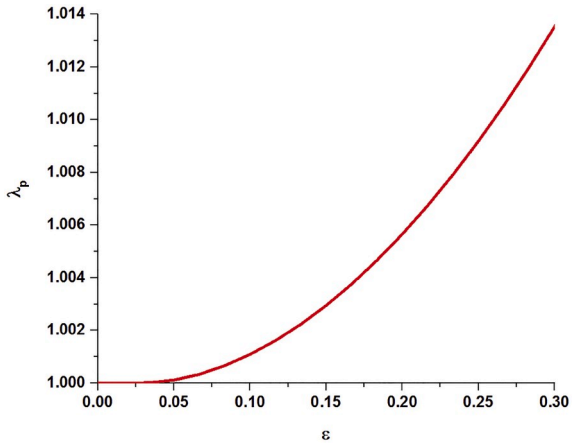

Fig. 4. The plastic stretching ratio corresponding to the nonlinear elastic-plastic stress-strain curve accounting for creep and viscoelastic relaxation predicted by Eqs. (35), (36) and (38). The result supplements that of Fig. 3.

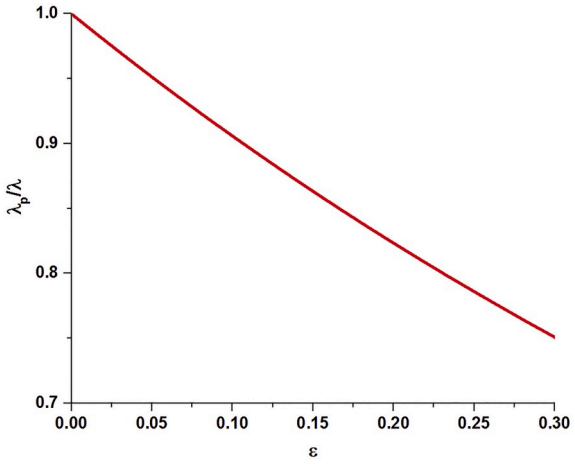

Fig. 5. The ratio λ_p/λ corresponding to the nonlinear elastic-plastic stress-strain curve accounting for creep and viscoelastic relaxation predicted by Eqs. (35), (36) and (38). The result supplements that of Fig. 3.

respectively.

3.3. Constitutive equation applied to creep and recovery tests

Let a fiber be fully unloaded at time t = 0 and then loaded practically instantaneously during a very short time $t_\ell \to 0$. Because the loading time is very short, according to Eq. (35) during such loading $\lambda_p \approx 1$. Let the loading happens with a very high rate of stretching $\dot{\varepsilon}_\ell \to \infty$, so that the strain $\varepsilon_\ell = \dot{\varepsilon}_\ell t_\ell$ is finite. Then, Eq. (38) yields

$$\sigma_0 \approx G\left(e^{\varepsilon_\ell}-e^{-2\varepsilon_\ell}\right) \tag{42}$$

The latter means that on the scale of the creeping and recovery test this initial stress σ_0 is applied at $t = t_\ell \approx 0$. In other words, in the creep and recovery test, at t = 0 the fiber is stretched instantaneously with a constant stress σ_0 and then during the time interval $0 < t \le t_1$ is held at this stress. Then, Eq. (37) yields for this time period the following dependence of strain on time

$$K(t)\left[\frac{\lambda^2(t)}{\lambda_p^2(t)}-\frac{\lambda_p(t)}{\lambda(t)}\right]=\frac{\sigma_0}{G}\left[1+\frac{(\gamma-\mu)}{\mu}\left(1-e^{-\mu t}\right)\right], \quad 0\le t\le t_1 \tag{43}$$

where

$$K(t)=\left\{1+4C_2'\left[\lambda^2(t)+\frac{2}{\lambda(t)}-3\right]+6C_3'\left[\lambda^2(t)+\frac{2}{\lambda(t)}-3\right]^2\right\} \tag{44}$$

Equation (43) with Eq. (44) yields the 9th order polynomial for λ(t)

$$k_{10}\lambda^9+k_8\lambda^7+k_7\lambda^6+k_6\lambda^5+k_5\lambda^4+k_4\lambda^3+k_3\lambda^2+k_2\lambda-24C_3'=0 \tag{45}$$

where the coefficients $k_{10}=6C_3'/\lambda_p^2$, $k_8=4C_2'/\lambda_p^2-36C_3'/\lambda_p^2$, $k_7=24C_3'/\lambda_p^2-6C_3'\lambda_p$, $k_6=1/\lambda_p^2-12C_2'/\lambda_p^2+54C_3'/\lambda_p^2 k_5=8C_2'/\lambda_p^2-4C_2'\lambda_p-72C_3'/\lambda_p^2+36C_3'\lambda_p$, $k_4=24C_3'/\lambda_p^2-24C_3'\lambda_p-D$, $k_3=-\lambda_p+12C_2'\lambda_p-54C_3'\lambda_p$, $k_2=-8C_2'\lambda_p+72C_3'\lambda_p$ and

$$D(t)=\frac{\sigma_0}{G}\left[1+\frac{(\gamma-\mu)}{\mu}(1-e^{-\mu t})\right] \tag{46}$$

It should be emphasized that all the above-mentioned coefficients are functions of time t, i.e., Eq. (45) should be solved at different time moments. For the values of the physical constants of interest in the present case, using Descarte's rule of signs [46], one should expect 5 or 3 or 1 positive real roots, which could have physical meaning. The numerical solution shows that there is only one real positive root λ(t).

In addition, Eqs. (35) and (36) provide the differential equation describing the plastic strain ratio $\lambda_p(t)$ in conjunction with Eqs. (43) and (44)

$$\frac{d\lambda_p}{dt}=\Gamma_0\exp\left[-\frac{1}{2}\left(\frac{Z}{\sigma_0}\right)^{2n}\right]\frac{\lambda_p\left(\lambda^3-\lambda_p^3\right)}{\left(\lambda^3+2\lambda_p^3\right)};\quad t=0,\quad \lambda_p=1 \tag{47}$$

It should be emphasized that strain is found as $\varepsilon=\ell n\lambda$.

After that, at $t=t_1$ the load is removed. At that moment of time the plastic stretching ratio reaches a certain value, which is denoted as

$$\lambda_{p\infty}=\lambda_p(t_1) \tag{48}$$

At $t>t_1$ the fiber stays unloaded and its viscoelastic recovery takes place. During the unloading process the plastic stretching ratio does not change anymore and stays equal to $\lambda_{p\infty}$. Then, Eq. (37) yields

$$K(t)\left[\frac{\lambda^2(t)}{\lambda_{p\infty}^2}-\frac{\lambda_{p\infty}}{\lambda(t)}\right]=\frac{\sigma_0}{G}\frac{(\gamma-\mu)}{\mu}(e^{-\mu(t-t_1)}-e^{-\mu t}),\quad t>t_1 \tag{49}$$

where

$$K(t)=\left\{1+4C_2'\left[\frac{\lambda^2(t)}{\lambda_{p\infty}^2}+2\frac{\lambda_{p\infty}}{\lambda(t)}-3\right]+6C_3'\left[\frac{\lambda^2(t)}{\lambda_{p\infty}^2}+2\frac{\lambda_{p\infty}}{\lambda(t)}-3\right]^2\right\} \tag{50}$$

Equation (49) with Eq. (50) yields the 9th order polynomial for λ(t)

$$k_{10}'\lambda^9+k_8'\lambda^7+k_7'\lambda^6+k_6'\lambda^5+k_5'\lambda^4+k_4'\lambda^3+k_3'\lambda^2+k_2'\lambda-24C_3'=0 \tag{51}$$

where $k_{10}=6C_3'/\lambda_{p\infty}^2$, $k_8=4C_2'/\lambda_{p\infty}^2-36C_3'/\lambda_{p\infty}^2$, $k_7=24C_3'/\lambda_{p\infty}^2-6C_3'\lambda_{p\infty}$, $k_6=1/\lambda_{p\infty}^2-12C_2'/\lambda_{p\infty}^2+54C_3'/\lambda_{p\infty}^2$, $k_5=8C_2'/\lambda_{p\infty}^2-4C_2'\lambda_{p\infty}-72C_3'/\lambda_{p\infty}^2+36C_3'\lambda_{p\infty}$, $k_4=24C_3'/\lambda_{p\infty}^2-24C_3'\lambda_{p\infty}-E$, $k_3=-\lambda_{p\infty}+12C_2'\lambda_{p\infty}-54C_3'\lambda_{p\infty}$, $k_2=-8C_2'\lambda_{p\infty}+72C_3'\lambda_{p\infty}$, with

$$E(t)=\frac{\sigma_0}{G}\frac{(\gamma-\mu)}{\mu}\left[e^{-\mu(t-t_1)}-e^{-\mu t}\right] \tag{52}$$

Equation (49) shows that as $t\to\infty$, the ratio $\lambda(t)/\lambda_{p\infty}\to1$, i.e. fiber deformation is irreversible, and a residual stretching $\lambda_{p\infty}$ is inevitably left. Because $\varepsilon=\ell n\lambda$, this means that the residual strain $\varepsilon_{p\infty}=\ell n\lambda_{p\infty}$ is present after the creep and recovery process in the cases when constant stress σ_0 was applied for a duration t_1.

The predicted result for the creep and recovery calculated using Eqs. (43)–(52) is presented in Fig. 6.

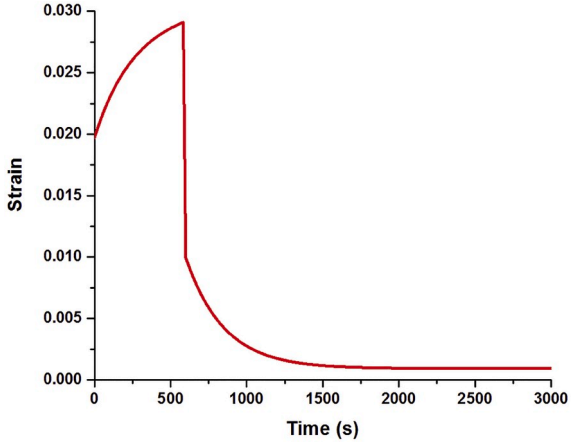

Fig. 6. Strain variation in time during the creep and viscoelastic recovery test predicted by Eqs. (43)–(52), with $\varepsilon=\ell n\lambda$. It is seen that the predicted residual strain is $\varepsilon_{p\infty}\approx0.001$ in this case. The following values of parameters were used: $\dot{\varepsilon}=0.001\,s^{-1}$, $\gamma=0.006\ s^{-1}$, $\mu=0.004\ s^{-1}$, E = 500 MPa, $C_2=200$ MPa, $C_3=10$ MPa, $\Gamma_0=0.0003\ s^{-1}$, Z = 20 MPa, n = 1, and $t_1=600$ s.

4. Comparison with experimental data and discussion

4.1. Nylon 6,6

4.1.1. Tensile behavior

Fig. 7 depicts the experimental results for nylon 6,6 specimens obtained in tensile tests. All of them reveal a nonlinear stress-strain dependence even at relatively low strains $\varepsilon<0.05$ (Fig. 7a). The rheological model reveals the results obtained from Eq. (40) [with Eq. (35) solved numerically subjected to the initial condition (36) using the Kutta-Merson method] with the strain rate of $10^{-5}\ s^{-1}$.

The values of the physical parameters of nylon established via fitting of the theory to the experiment in Fig. 7 are listed in Table 2. Nylon 6,6 shows a characteristic nonlinear stress-strain curve at high strains as observed for rubber [7]. The material constants Γ_0, Z and n determine the plastic behavior of the fiber as explained before. It should be emplasized that an ideal plastic behavior would not reveal the characteristic increase in stress after plasticity sets in, as it observed in Fig. 7. The increase in the stress in the nonlinear regime is affected by the physical hyperelastic parameters C_2 and C_3, as well as the non-ideal plasticity.

4.1.2. Behavior in creep and recovery

In the present experiments, fiber-like specimens were loaded for $t_1=600$ s with a certain tensile stress σ_0 to observe fiber creep. Then, the specimens were unloaded and observed up to 6000 s to trace fiber recovery. Fig. 8 depicts the experimental data obtained for the stress range $\sigma_0=20$–160 MPa. The theoretical predictions employed the same set of material parameters, as those found in the tensile test and listed in Table 2.

It can be seen that the theoretical model can accurately predict the material behavior in both tensile and creep and recovery tests with the same set of parameters. The time-dependent change in strain observed in the recovery tests for all stresses σ_0 reveals the effect of the viscoelastic nature of the material. At the end of the recovery stage at t = 6600 s, which is a practical infinity, way beyond the time-dependent viscoelastic recovery, there is still a non-zero residual strain for all cases. This is the manifestation of the plasticity of the polymer specimens, and the rheological model does captures this residual strain.

4.1.3. Comparison for different strains

In each experiment of Fig. 8 the residual plastic strain $\varepsilon_{p\infty}$ has been measured at the end of the test (which is essentially long after the

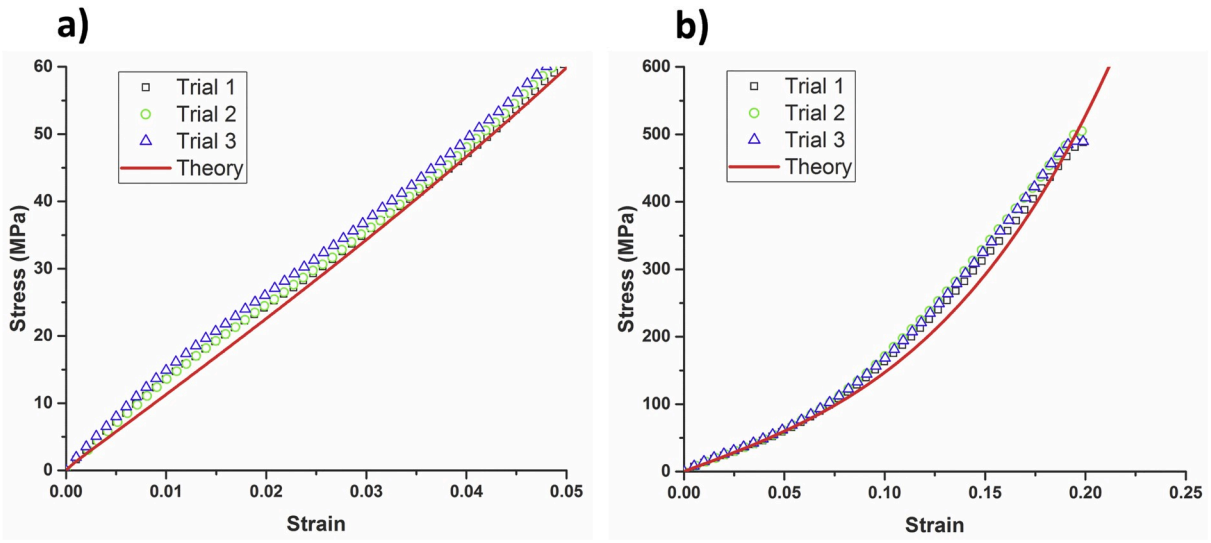

Fig. 7. Stress-strain curves for nylon 6,6 specimens measured in tensile tests at the stretching rate of 0.006 mm/min: (a) until a moderate strain of $\varepsilon = 0.05$, and (b) until the ultimate strength and failure. True stress and strains are plotted for the experimental values and the theory. Relative Humidity (RH) = 60–70%. The experimental data are shown by symbols, whereas the theoretical predictions – by lines.

Table 2
Material parameters of nylon 6,6 fiber-like specimen established in tensile tests.

γ (s^{-1})	μ (s^{-1})	E (MPa)	C_2 (MPa)	C_3 (MPa)	Γ_0(s^{-1})	Z (MPa)	n
0.016	0.01	1580	1400	210	0.000016	20	1

viscoelastic recovery). It is plotted versus the initial elastic strain in Fig. 9. The difference between the maximum strain ε_{max} (after the creep stage) and the initial elastic strain, i.e., $\varepsilon_{max} - \varepsilon_0$, is plotted against the initial elastic strain in Fig. 10. These residual plastic strains are important for design considerations and would not be revealed by tensile tests alone.

The residual plastic strain observed in Fig. 9 is relatively smaller than

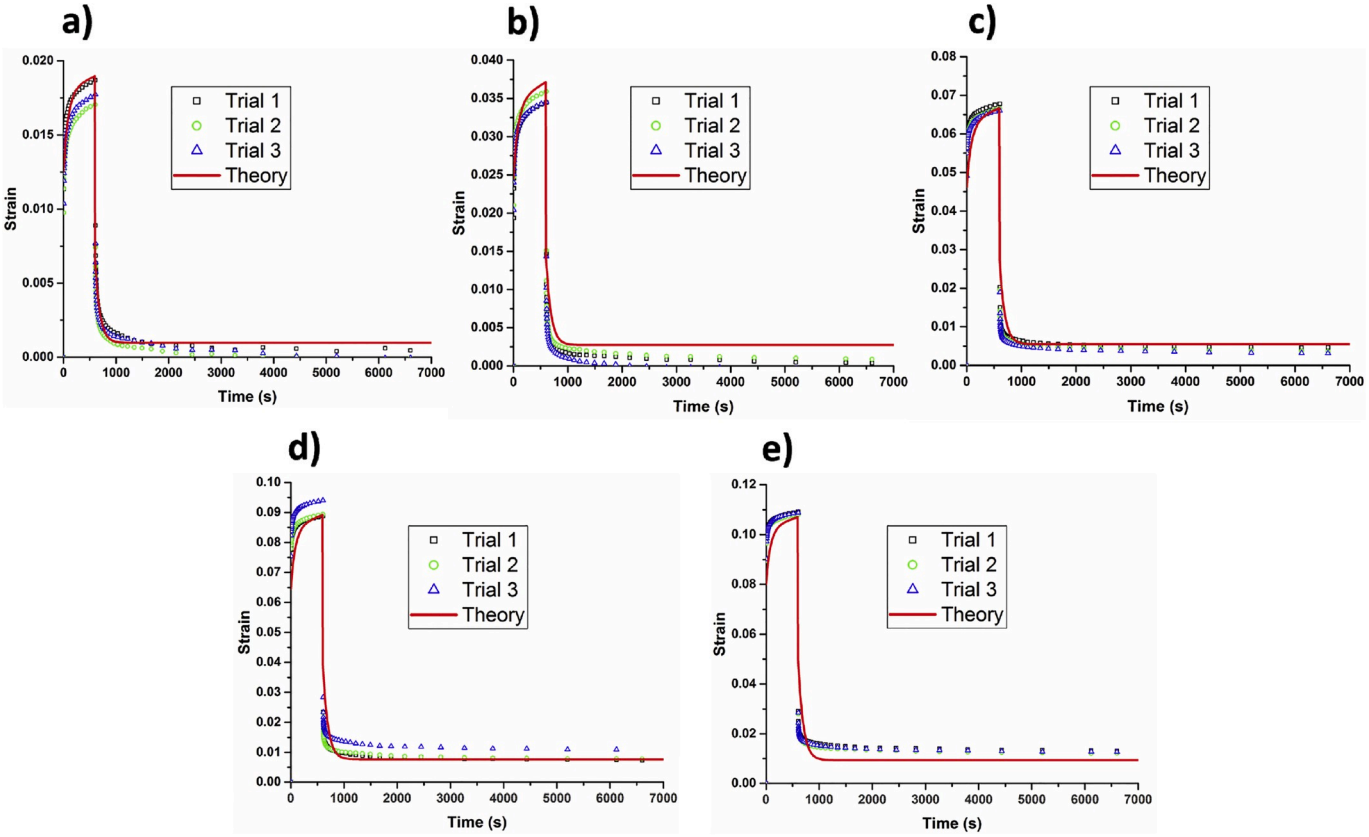

Fig. 8. Comparison of the theoretical predictions and experiments in the creep and recovery tests of nylon 6,6 specimens stretched at (a) $\sigma_0 = 20$ MPa, (b) $\sigma_0 = 40$ MPa, (c) $\sigma_0 = 80$ MPa, (d) $\sigma_0 = 120$ MPa, and (e) $\sigma_0 = 160$ MPa for 600 s, and then recovered. RH = 60–70%. The experimental data are shown by symbols, whereas the theoretical predictions – by lines.

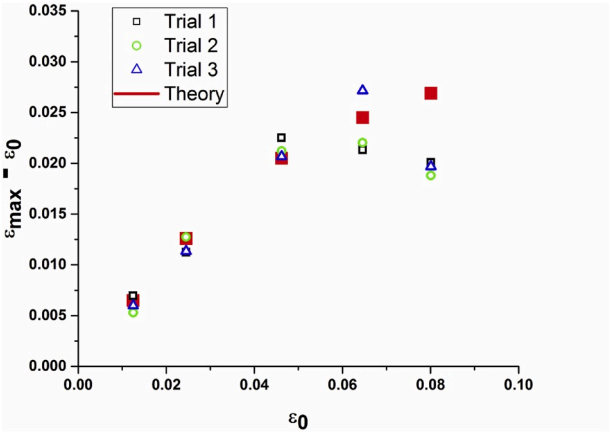

Fig. 9. Plastic strain $\varepsilon_{p\infty}$ versus the elastic strain ε_0 for nylon 6,6 specimens at different stresses $\sigma_0 = 20$, 40, 80, 120 and 160 MPa.

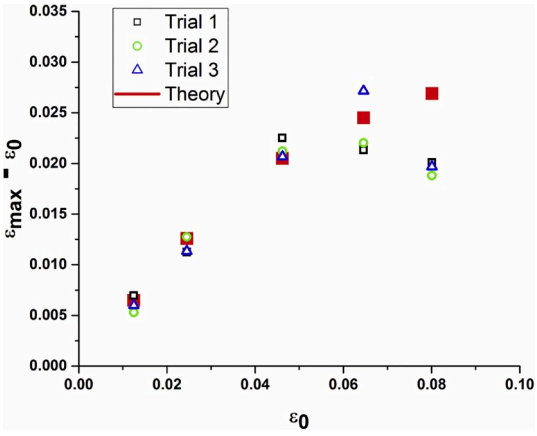

Fig. 10. The strain difference $\varepsilon_{max} - \varepsilon_0$ versus the elastic strain ε_0 for nylon 6,6 specimens at different stresses $\sigma_0 = 20$, 40, 80, 120 and 160 MPa.

the elastic strain at the stresses $\sigma_0 = 20$ MPa and $\sigma_0 = 40$ MPa. However, the residual plastic strain increases considerably at high stresses, for example, for $\sigma_0 = 80$ MPa the residual plastic strain is about 9% of the elastic strain, and for $\sigma_0 = 160$ MPa the residual plastic strain is about 16% of the elastic strain. Additionally, Fig. 10, shows that the maximum strain observed at the end of 600 s is about 1.5 times the elastic strain for the stresses $\sigma_0 = 20$–80 MPa, while it reduces to about 1.4 times and 1.25 times at 120 MPa and 160 MPa, respectively.

4.2. Polyethylene terephthalate (PET)

4.2.1. Tensile behavior

Fig. 11 depicts the experimental results for polyethylene terephthalate (PET) specimens obtained in tensile tests. All of them reveal a nonlinear stress-strain dependence even at relatively low strains $\varepsilon < 0.05$ (Fig. 11). The material parameters found are listed in Table 3. It should be emphasized that the model performance is satisfactory up to the strain $\varepsilon \approx 0.06$. At higher strains the model with the chosen values of parameters listed in Table 3 under-predicts the stress values. The parameters are chosen to be uniformly valid for tensile test considered in this sub-section and the creep and recovery tests considered in sub-section 4.2.2. A better fitting of the model in the $\varepsilon > 0.06$ range would cause a deteriorated accuracy in the creep and recovery tests. Accordingly, the chosen parameter values serve as the best uniformly valid set possible for the present phenomenological model.

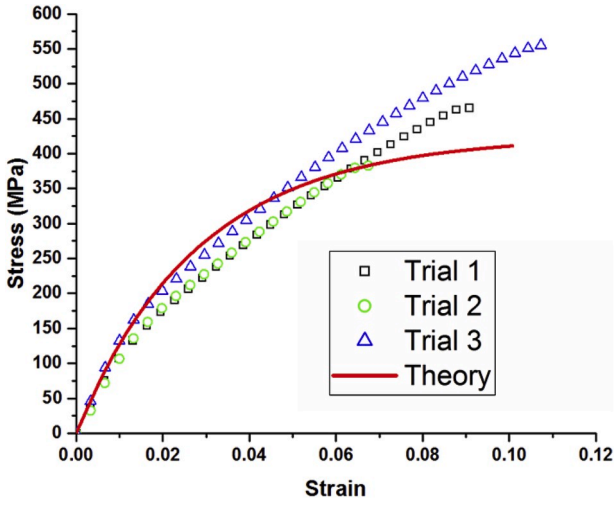

Fig. 11. True stress-true strain curves for polyethylene terephthalate (PET) fiber specimens measured in tensile tests at the stretching rate of 100 μm/min. RH = 16–21% The experimental data are shown by symbols, whereas the theoretical predictions – by line.

Table 3
Material parameters of PET fiber specimen established with the model.

γ (s^{-1})	μ (s^{-1})	E (MPa)	C_2 (MPa)	C_3 (MPa)	Γ_0(s^{-1})	Z (MPa)	n
0.0058	0.005	13800	10	10	0.0048	80	1

4.2.2. Behavior in creep and recovery

Fig. 12 shows the experimental results for PET obtained in creep and recovery tests at stresses 40–160 MPa. It is observed that the PET fiber behavior in creep and recovery are accurately predicted with the uniformly valid set of parameters in Table 3. There is a significant under-prediction of the creep strain at 160 MPa. This is an inevitable consequence of the uniformly valid set of the physical parameters chosen for PET for the present phenomenological model.

4.3. Polybutylene terephthalate (PBT)

4.3.1. Tensile behavior

Fig. 13 shows the experimental results for polybutylene terephthalate (PBT) specimens obtained in tensile tests. The results reveal a stress-strain dependence like the one for an elastic-plastic material at relatively low strains $\varepsilon < 0.05$. However, at higher strains, PBT reveals a characteristic nonlinear stress-strain curve as observed for rubber [7]. The material parameters of the rheological constitutive equation established in conjunction to these experiments are listed in Table 4. The theoretical model over-predicts the stress at higher strains (>0.27). This might be related to the mechanical degradation in polymers at high stresses which is not accounted for in the present phenomenological model.

4.3.2. Behavior in creep and recovery

It is observed that in the creep-recovery experiments presented in Fig. 14, the rheological model accurately predicts the PBT fiber deformation in the cases of 20 MPa and 40 MPa with the same set of material parameters as that for the tensile test (Table 4). However, at higher stresses employed in the creep tests, the model underpredicts the deformation considerably. It is interesting to note that the description of the strain in creep deteriorates at higher stretching stresses, which shows that the constant uniformly valid physical parameters of the present phenomenological model probably fail due to the fact that the elastic modulus can diminish at higher stresses, for example, due to the

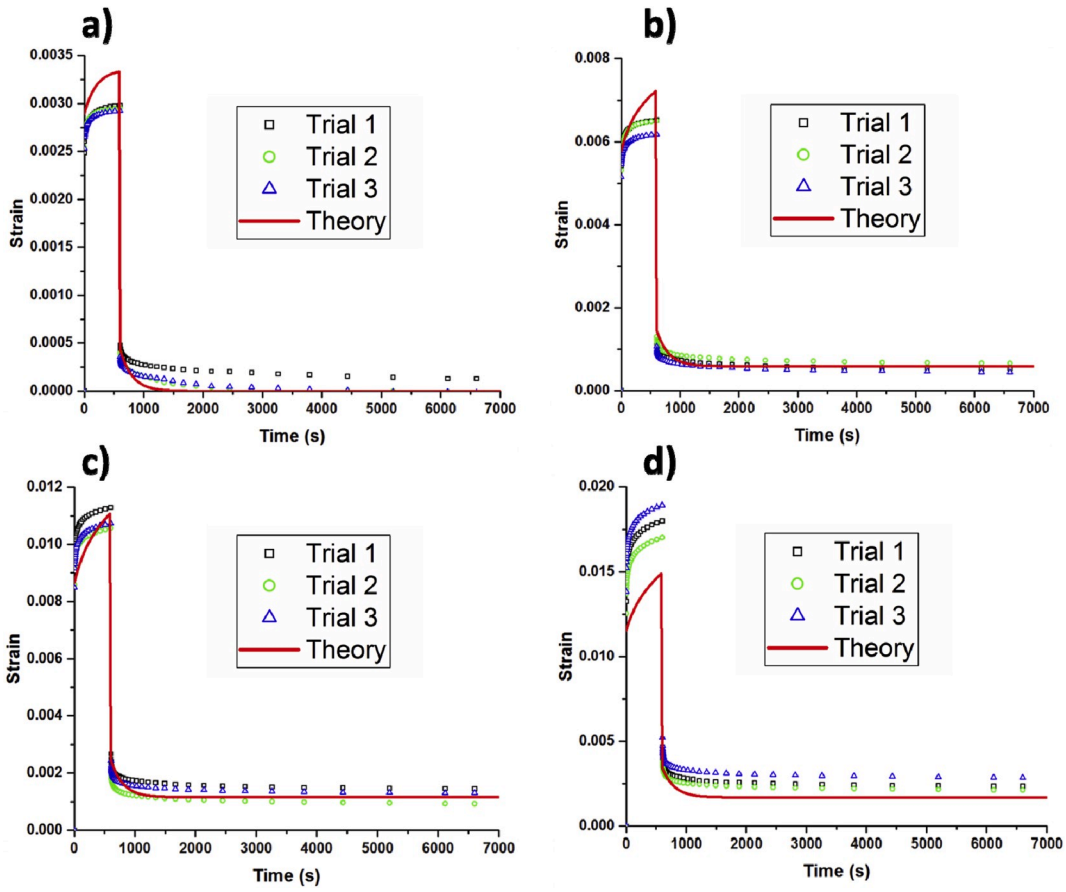

Fig. 12. Comparison of the theoretical predictions and experiments in the creep and recovery tests of PET fiber stretched at (a) $\sigma_0 = 40$ MPa, (b) $\sigma_0 = 80$ MPa, (c) $\sigma_0 = 120$ MPa, and (d) $\sigma_0 = 160$ MPa for 600 s, and then recovered. RH = 16–21%. The experimental data are shown by symbols, whereas the theoretical predictions – by lines.

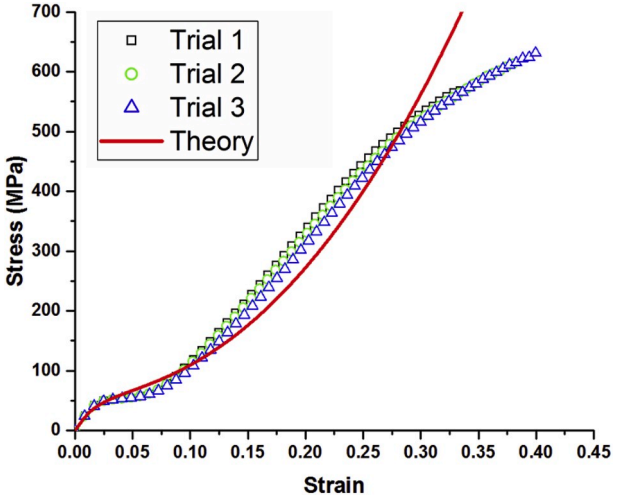

Fig. 13. True stress-true strain curves for PBT fiber specimens measured in tensile tests at the stretching rate of 100 μm/min. RH = 16–21%. The experimental data are shown by symbols, whereas the theoretical predictions – by line.

mechanical degradation.

Fig. 15 shows the comparison with the change in the elastic and viscoplastic material parameters to those listed in Table 5. It is seen that the rheological model better captures the fiber behavior in the creep and recovery tests at 80 MPa, 120 MPa and 160 MPa with this set of parameters, albeit being already not a uniformly valid one.

Table 4
Material parameters of PBT fiber specimen.

γ (s^{-1})	μ (s^{-1})	E (MPa)	C_2 (MPa)	C_3 (MPa)	Γ_0(s^{-1})	Z (MPa)	n
0.008	0.0065	2700	7500	2.5	0.0075	30	1

4.4. Polypropylene

4.4.1. Polypropylene: tensile behavior

The experimental results for polypropylene specimens obtained in tensile tests are shown in Fig. 16. The model results are obtained with the strain rate of 1.67×10^{-4} s^{-1} with the corresponding material parameters listed in Table 6. The experimental results deviate from each other slightly at higher strains, and the theoretical model reveals an increase in stress at strains $\varepsilon > 0.20$ in comparison to the experimental results. As mentioned before, this might be related to the mechanical degradation in polymers at high stresses which is not accounted for in the present phenomenological model.

4.4.2. Polypropylene: Behavior in creep and recovery

Experimental results and model prediction obtained for creep and recovery tests with the creep stress between 20 MPa and 160 MPa are shown in Fig. 17. It is evident that the theoretical model can predict the material behavior in both tensile and creep and recovery tests with the same set of parameters with only minor deviations. However, at the creep stresses in the 80 MPa–160 MPa range, the model under-predicts

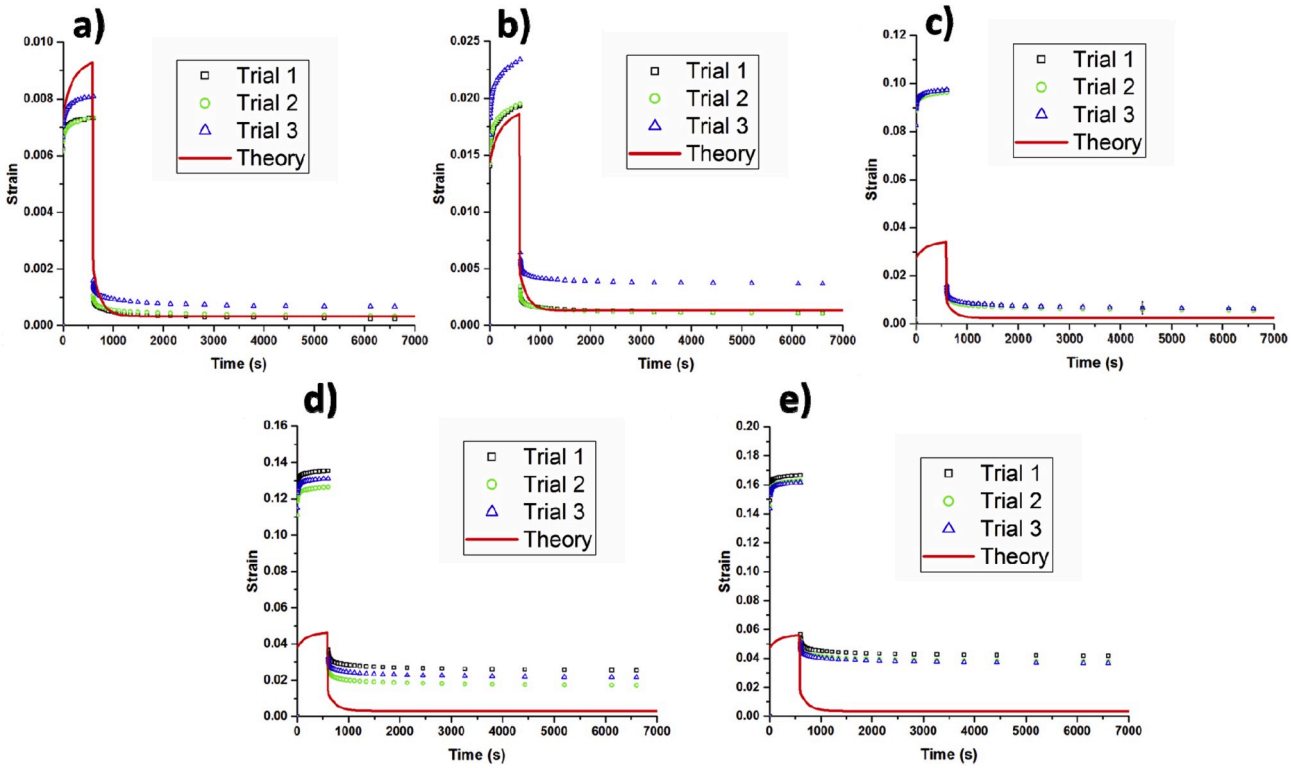

Fig. 14. Comparison of the theoretical predictions and experiments in the creep and recovery tests of PBT fiber stretched at (a) $\sigma_0 = 20$ MPa, (b) $\sigma_0 = 40$ MPa, (c) $\sigma_0 = 80$ MPa, (d) $\sigma_0 = 120$ MPa, and (e) $\sigma_0 = 160$ MPa for 600 s, and then recovered. RH = 16–21%. The experimental data are shown by symbols, whereas the theoretical predictions – by lines.

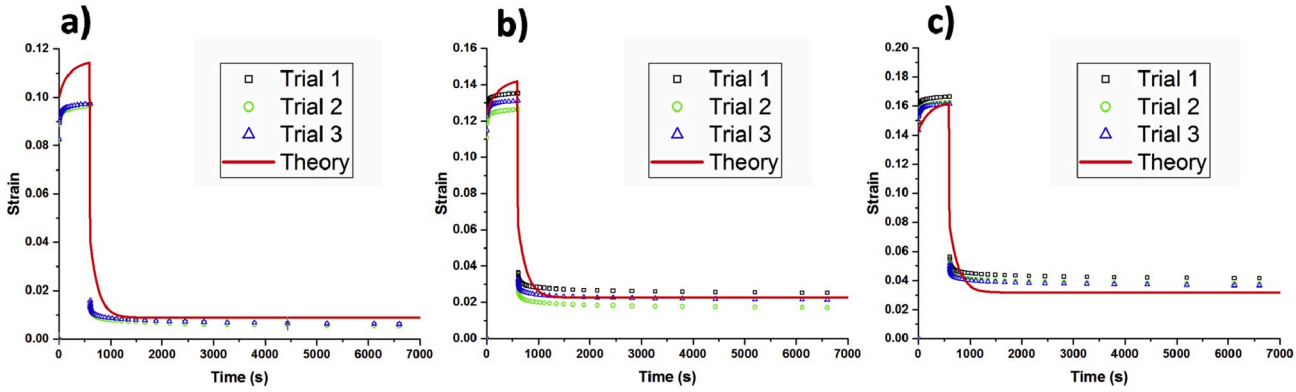

Fig. 15. Comparison of the theoretical predictions and experiments with the change in the material parameters as in Table 5 for PBT fiber stretched at (a) $\sigma_0 = 80$ MPa, (b) $\sigma_0 = 120$ MPa, and (c) $\sigma_0 = 160$ MPa for 600 s, and then recovered. The experimental data are shown by symbols, whereas the theoretical predictions – by lines.

Table 5
Modified material parameters of PBT fiber specimen.

γ (s^{-1})	μ (s^{-1})	E (MPa)	C_2 (MPa)	C_3 (MPa)	Γ_0(s^{-1})	Z (MPa)	n
0.008	0.0065	500	700	2.5	0.0018	140	1

strains during the creep test, probably due to the mechanical degradation unaccounted for by the present phenomenological model.

4.5. Polytetrafluoroethylene

4.5.1. Polytetrafluoroethylene: tensile behavior

Fig. 18 depicts the experimental results for polytetrafluoroethylene (PTFE) specimens obtained in the tensile tests. The results revealed viscoelastic-plastic deformation with a pronounced plastic deformation. The fibers did not reach their breaking point in the results shown in Fig. 18. The material parameters corresponding to the rheological model fitting to these data are listed in Table 7.

4.5.2. Polytetrafluoroethylene: Behavior in creep and recovery

Experimental results and model prediction obtained for creep and recovery tests with creep stress between 10 MPa and 40 MPa are shown in Fig. 19. The theoretical results are based on the material parameters listed in Table 7. The model captures the creep-recovery deformation satisfactorily. However, the description deteriorates at the stress of 40 MPa, probably because of the unaccounted for mechanical degradation.

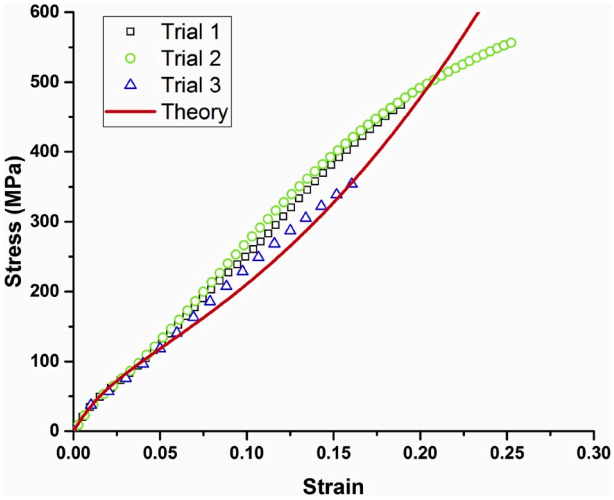

Fig. 16. True stress-true strain curves for polypropylene fiber specimens measured in tensile tests at the stretching rate of 100 μm/min. RH = 21–25%. The experimental data are shown by symbols, whereas the theoretical predictions – by line.

Table 6
Material parameters of polypropylene fiber.

γ (s^{-1})	μ (s^{-1})	E (MPa)	C_2 (MPa)	C_3 (MPa)	Γ_0(s^{-1})	Z (MPa)	n
0.016	0.01	4020	4000	14	0.0022	40	1

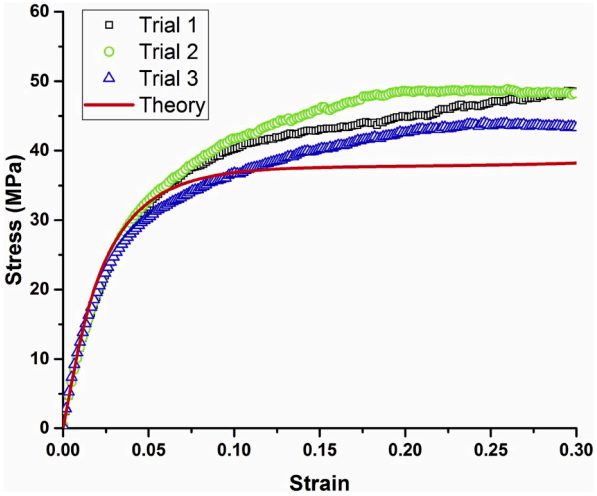

Fig. 18. True stress-true strain curves for polytetrafluoroethylene fiber specimens measured in tensile tests at the stretching rate of 100 μm/min. RH = 24–27%. The experimental data are shown by symbols, whereas the theoretical predictions – by line.

Table 7
Material parameters of polytetrafluoroethylene fiber specimen.

γ (s^{-1})	μ (s^{-1})	E (MPa)	C_2 (MPa)	C_3 (MPa)	Γ_0(s^{-1})	Z (MPa)	n
0.013	0.010	1360	1	11	0.0054	20	1

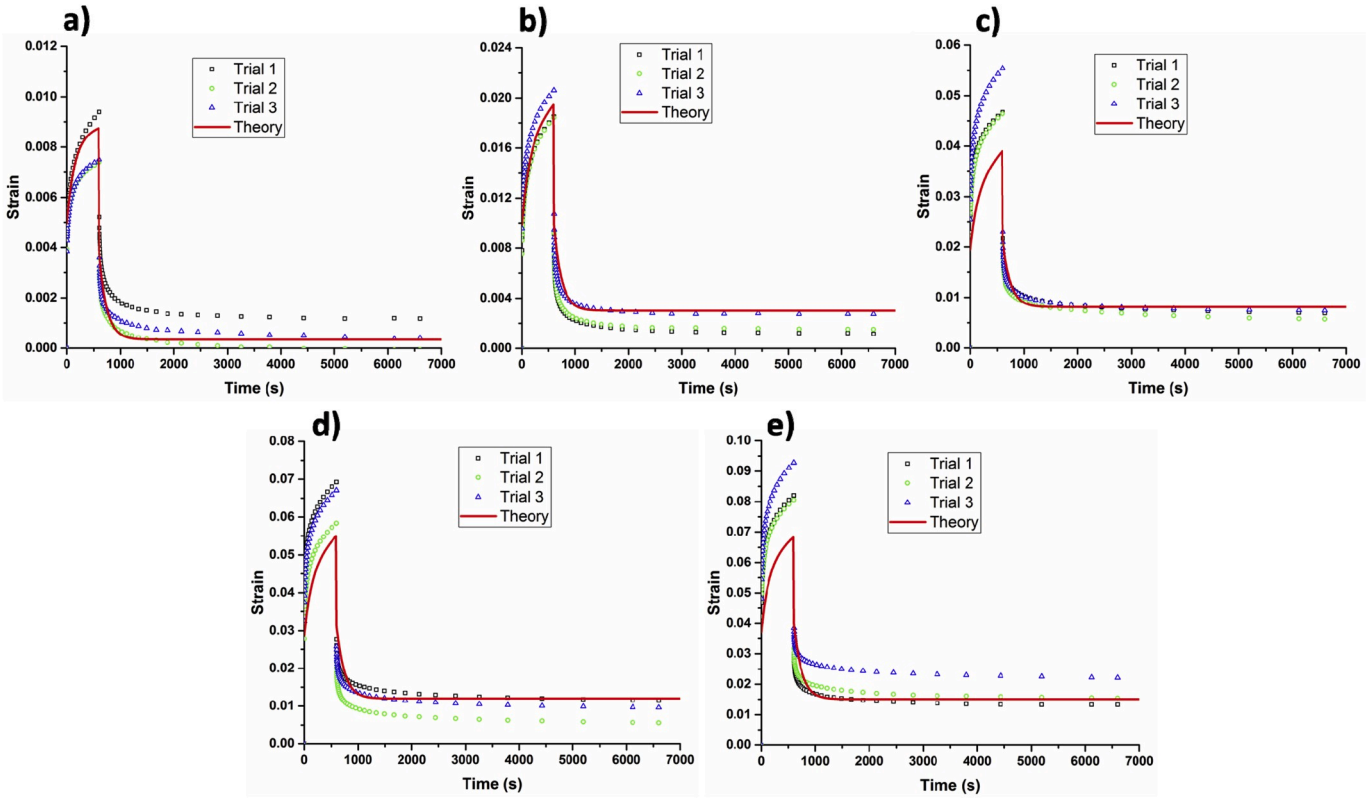

Fig. 17. Comparison of the theoretical predictions and experiments in the creep and recovery tests of polypropylene fiber stretched at (a) σ_0 = 20 MPa, (b) σ_0 = 40 MPa, (c) σ_0 = 80 MPa, (d) σ_0 = 120 MPa, and (e) σ_0 = 160 MPa for 600 s, and then recovered. RH = 21–25%. The experimental data are shown by symbols, whereas the theoretical predictions – by lines.

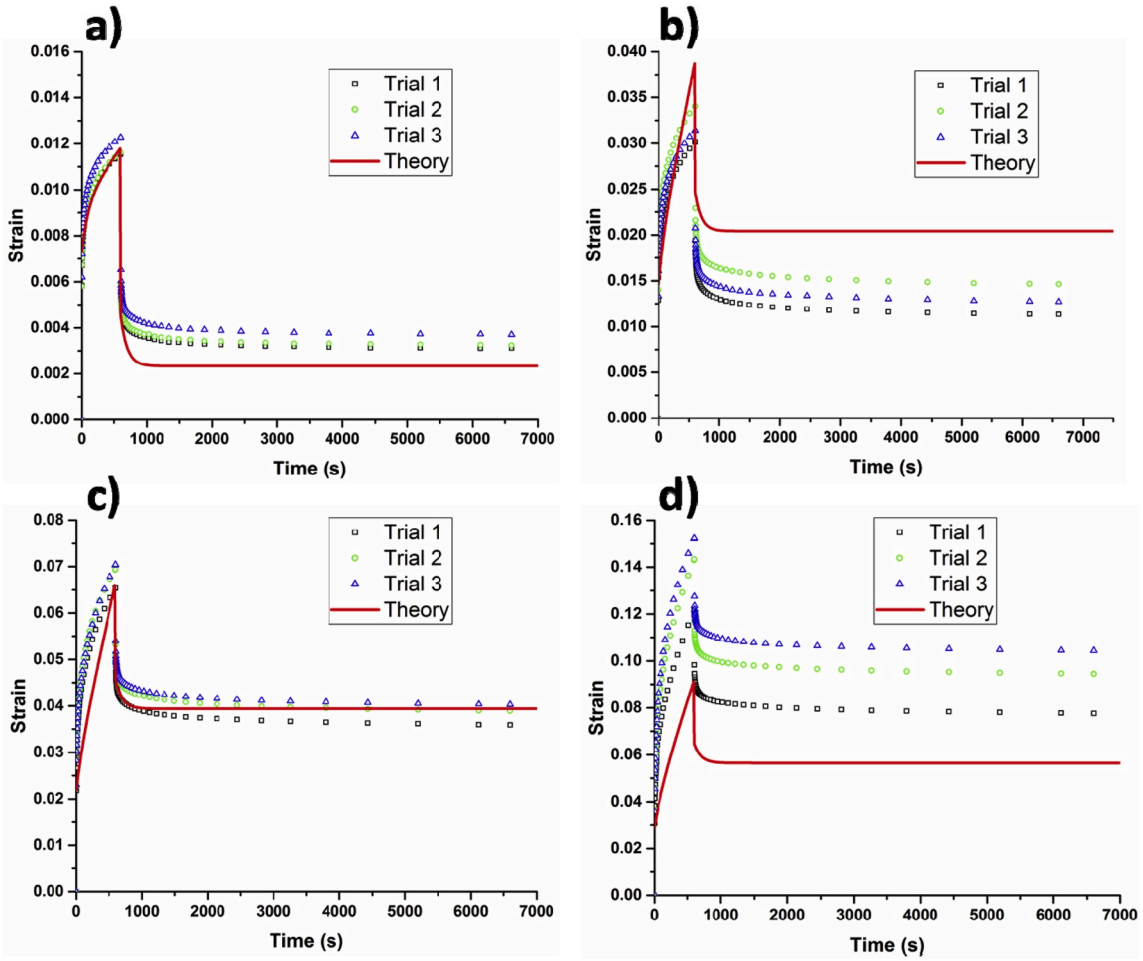

Fig. 19. Comparison of the theoretical predictions and experiments in the creep and recovery tests of polytetrafluoroethylene fiber stretched at (a) $\sigma_0 = 10$ MPa, (b) $\sigma_0 = 20$ MPa, (c) $\sigma_0 = 30$ MPa, and (d) $\sigma_0 = 40$ MPa for 600 s, and then recovered. RH = 24–27%. The experimental data are shown by symbols, whereas the theoretical predictions – by lines.

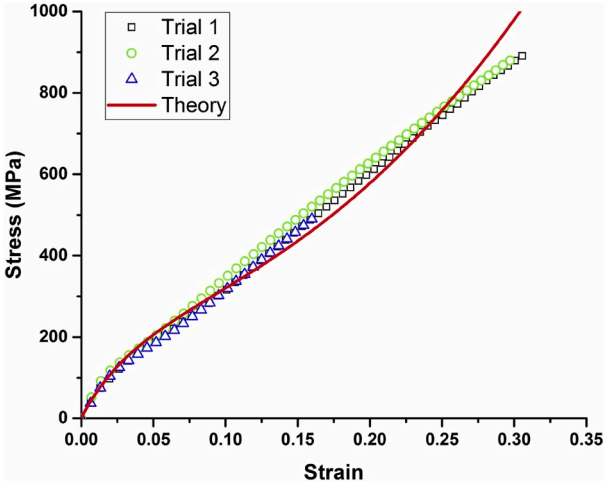

Fig. 20. True stress-true strain curves for polyethyletherketone fiber specimens measured in tensile tests at the stretching rate of 100 μm/min. RH = 24–27%. The experimental data are shown by symbols, whereas the theoretical predictions – by line.

4.6. Polyethyletherketone

4.6.1. Polyethyletherketone: tensile behavior

Fig. 20 depicts the experimental results for polyethyletherketone (PEEK) specimens obtained in tensile tests. The deviation of the predictions from the experimental data at higher stresses and strains can be caused by the mechanical degradation unaccounted for by the phenomenological model. The material parameters corresponding to fitting of the rheological model to the data are listed in Table 8.

4.6.2. Polyethyletherketone: Behavior in creep and recovery

It is observed that in comparison with the results of the creep-recovery experiments presented in Fig. 21, the model accurately predicts the PEEK fiber deformation in case of 20 MPa–80 MPa. At higher creep stresses of 120 MPa and 160 MPa, the model underpredicts the deformation at the creep stage. However, the residual plastic strain is satisfactorily predicted for all cases. The experimental results at 120 MPa and 160 MPa indicate an apparent reduction in the elastic modulus due to the mechanical degradation unaccounted for by the present

Table 8
Material parameters of polyethyletherketone fiber specimen established in tensile tests.

γ (s^{-1})	μ (s^{-1})	E (MPa)	C_2 (MPa)	C_3 (MPa)	Γ_0(s^{-1})	Z (MPa)	n
0.012	0.010	7000	4500	10	0.0035	5	1

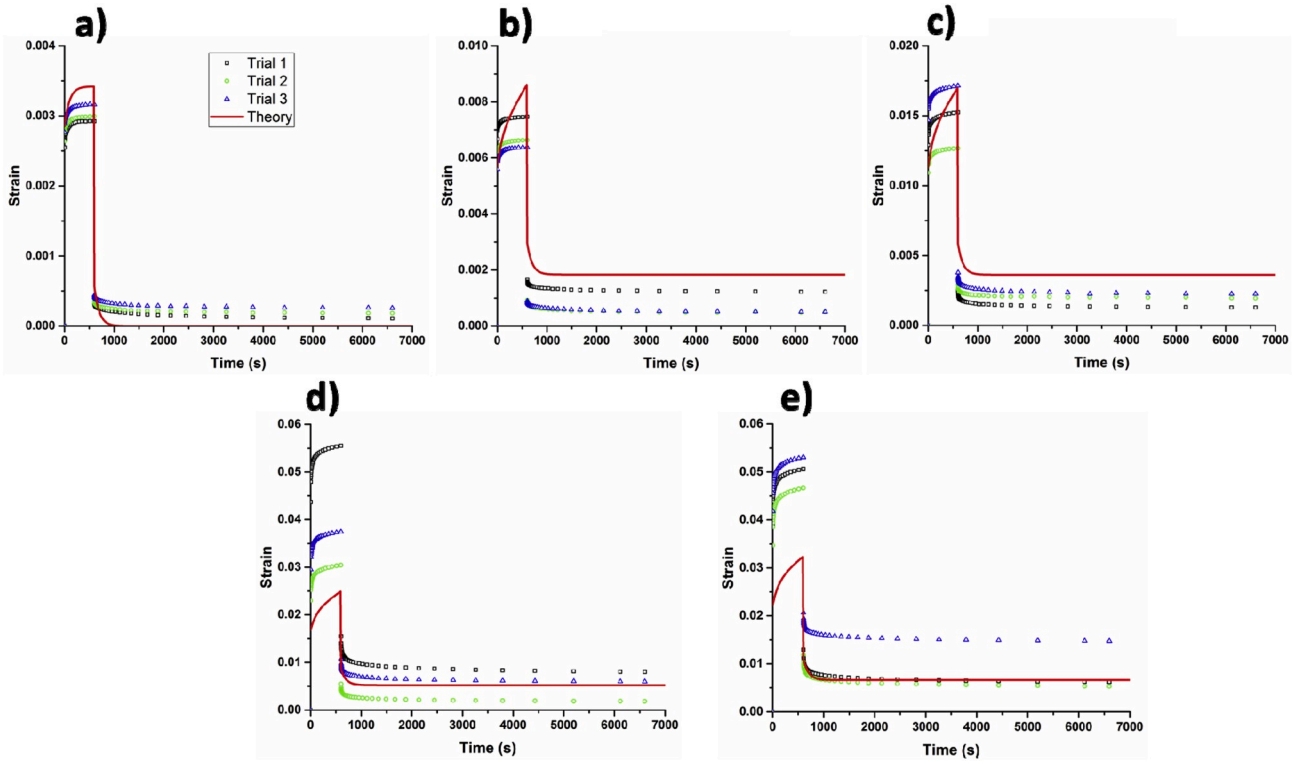

Fig. 21. Comparison of the theoretical predictions and experiments in the creep and recovery tests of polyethyletherketone (PEEK) fiber stretched at (a) $\sigma_0 = 20$ MPa, (b) $\sigma_0 = 40$ MPa, (c) $\sigma_0 = 80$ MPa, (d) $\sigma_0 = 120$ MPa, and (e) $\sigma_0 = 160$ MPa for 600 s, and then recovered. RH = 24–27%. The experimental data are shown by symbols, whereas the theoretical predictions – by lines.

phenomenological model.

5. Conclusion

A comprehensive phenomenological constitutive model accounting for hyperelastic, plastic, creep and viscoelastic behavior of elastomers is proposed. The rheological model reveals all the characteristics, which are observed experimentally. Tensile, creep and recovery experiments were conducted with such specimens as nylon 6,6, polyethylene terephthalate, polybutylene terephthalate, polypropylene, polytetrafluoroethylene and polyethyletherketone. The phenomenological model was compared with these experiments. With uniformly valid material parameters, the model proposed in this work predicted the stress-strain curve in tensile tests with large deformations, as well as creep and subsequent viscoelastic recovery except in the case of PBT. Also, the model was able to predict the measured maximum and residual plastic strains resulting from the creep and recovery tests. Considerable change in the elastic and viscoplastic material parameters was required in the case of polybutylene terephthalate (PBT) to model the creep-recovery behavior.

Declaration of competing interest

The authors certify that this project has no conflict of interest.

CRediT authorship contribution statement

Alexander L. Yarin: Conceptualization, Methodology, Formal analysis, Resources, Writing - original draft, Writing - review & editing, Supervision, Project administration, Funding acquisition. **Abhilash Sankaran:** Methodology, Software, Validation, Formal analysis, Investigation, Data curation, Writing - original draft, Writing - review & editing. **Seongpil An:** Methodology, Validation, Formal analysis, Investigation, Data curation, Writing - original draft, Writing - review & editing. **Behnam Pourdeyhimi:** Conceptualization, Resources, Writing - original draft, Writing - review & editing, Supervision, Funding acquisition.

Acknowledgement

This work is supported by the Nonwovens Institute, U.S.A, grant No. 17-206.

References

[1] L.D. Landau, E.M. Lifshitz, Theory of Elasticity, Pergamon, Oxford, 1970.
[2] A.I. Lurie, Theory of Elasticity, Springer, Heidelberg, 2005.
[3] W. Brostow, E.H. Hagg Lobland, Materials: Introduction and Applications, John Wiley & Sons, Hoboken, 2017.
[4] L.R.G. Treloar, The Physics of Rubber Elasticity, Oxford University Press, Oxford, 1975.
[5] M. Mooney, A theory of large elastic deformation, J. Appl. Phys. 11 (1940) 582–592.
[6] P.J. Blatz, W.L. Ko, Application of finite elastic theory to the deformation of rubbery materials, Trans. Soc. Rheol. 6 (1962) 223–252.
[7] O.H. Yeoh, Some forms of the strain energy function for rubber, Rubber Chem. Technol. 66 (1993) 754–771.
[8] A.H. Muhr, Modeling the stress-strain behavior of rubber, Rubber Chem. Technol. 78 (2005) 391–425.
[9] M. Rachik, D. Barthes-Biesel, M. Carin, F. Edwards-Levy, Identification of the elastic properties of an artificial capsule membrane with the compression test: effect of thickness, J. Colloid Interface Sci. 301 (2006) 217–226.
[10] V. Kanyanta, A. Ivankovic, Mechanical characterisation of polyurethane elastomer for biomedical applications, J. Mech. Behav. Biomed. Mater. 3 (2010) 51–62.
[11] L.M. Kachanov, Fundamentals of the Theory of Plasticity, Dover Publ., New York, 2004.
[12] Y.N. Rabotnov, Creep Problems in Structural Members, North-Holland Publishing Company, Amsterdam, 1969.
[13] A. Khan, H. Zhang, Finite deformation of a polymer: experiments and modeling, Int. J. Plast. 17 (2001) 1167–1188.
[14] A. Benatar, D. Rittel, A.L. Yarin, Theoretical and experimental analysis of longitudinal wave propagation in cylindrical viscoelastic rods, J. Mech. Phys. Solid. 51 (2003) 1413–1431.

[15] A.S. Khan, O. Lopez-Pamies, R. Kazmi, Thermo-mechanical large deformation response and constitutive modeling of viscoelastic polymers over a wide range of strain rates and temperatures, Int. J. Plast. 22 (2006) 581–601.
[16] A.S. Khan, B. Farrokh, Thermo-mechanical response of nylon 101 under uniaxial and multi-axial loadings: Part I, Experimental results over wide ranges of temperatures and strain rates, Int. J. Plast. 22 (2006) 1506–1529.
[17] A.L. Yarin, I.V. Roisman, C. Tropea, Collision Phenomena in Liquids and Solids, Cambridge University Press, Cambridge, 2017.
[18] V. Srivastava, S.A. Chester, L. Anand, Thermally actuated shape-memory polymers: experiments, theory, and numerical simulations, J. Mech. Phys. Solid. 58 (2010) 1100–1124.
[19] A. Maurel-Pantel, E. Baquet, J. Bikard, J.L. Bouvard, N. Billon, A thermo-mechanical large deformation constitutive model for polymers based on material network description: application to a semi-crystalline polyamide 66, Int. J. Plast. 67 (2015) 102–126.
[20] A. Launay, M.H. Maitournam, Y. Marco, I. Raoult, F. Szmytka, Cyclic behaviour of short glass fibre reinforced polyamide: experimental study and constitutive equations, Int. J. Plast. 27 (2011) 1267–1293.
[21] A.K. Shojaei, A.R. Wedgewood, An anisotropic cyclic plasticity, creep and fatigue predictive tool for unfilled polymers, Mech. Mater. 106 (2017) 20–34.
[22] R. Boyd, G. Smith, Polymer Dynamics and Relaxation, Cambridge University Press, Cambridge, 2007.
[23] D. Hossain, M.A. Tschopp, D.K. Ward, J.L. Bouvard, P. Wang, M.F. Horstemeyer, Molecular dynamics simulations of deformation mechanisms of amorphous polyethylene, Polymer 51 (2010) 6071–6083.
[24] S. Yang, S. Yu, J. Ryu, J.M. Cho, W. Kyoung, D.S. Han, M. Cho, Nonlinear multiscale modeling approach to characterize elastoplastic behavior of CNT/polymer nanocomposites considering the interphase and interfacial imperfection, Int. J. Plast. 41 (2013) 124–146.
[25] D. Garcia-Gonzalez, A. Rusinek, T. Jankowiak, A. Arias, Mechanical impact behavior of polyether–ether–ketone (PEEK), Compos. Struct. 124 (2015) 88–99.
[26] A. Dorfmann, R.W. Ogden, A constitutive model for the Mullins effect with permanent set in particle-reinforced rubber, Int. J. Solid Struct. 41 (2004) 1855–1878.
[27] E. Krempl, K. Ho, An overstress model for solid polymer deformation behavior applied to Nylon 66, in: Time Dependent and Nonlinear Effects in Polymers and Composites, ASTM International, 2000.
[28] G. Ayoub, F. Zaïri, M. Naït-Abdelaziz, J.M. Gloaguen, Modeling the low-cycle fatigue behavior of visco-hyperelastic elastomeric materials using a new network alteration theory: application to styrene-butadiene rubber, J. Mech. Phys. Solid. 59 (2011) 473–495.
[29] Q. Guo, F. Zaïri, X. Guo, A thermo-viscoelastic-damage constitutive model for cyclically loaded rubbers. Part I: model formulation and numerical examples, Int. J. Plast. 101 (2018) 106–124.
[30] S. Fahimi, M. Baghani, M.R. Zakerzadeh, A. Eskandari, Developing a visco-hyperelastic material model for 3D finite deformation of elastomers, Finite Elem. Anal. Des. 140 (2018) 1–10.
[31] F. Chen, R. Balieu, N. Kringos, Thermodynamics-based finite strain viscoelastic-viscoplastic model coupled with damage for asphalt material, Int. J. Solid Struct. 129 (2017) 61–73.
[32] A. Shojaei, G. Li, Viscoplasticity analysis of semicrystalline polymers: a multiscale approach within micromechanics framework, Int. J. Plast. 42 (2013) 31–49.
[33] M. Ponçot, F. Addiego, A. Dahoun, True intrinsic mechanical behaviour of semi-crystalline and amorphous polymers: influences of volume deformation and cavities shape, Int. J. Plast. 40 (2013) 126–139.
[34] G.Z. Voyiadjis, A. Shojaei, N. Mozaffari, Strain gradient plasticity for amorphous and crystalline polymers with application to micro-and nano-scale deformation analysis, Polymer 55 (2014) 4182–4198.
[35] G. Ayoub, F. Zaïri, M. Naït-Abdelaziz, J.M. Gloaguen, Modelling large deformation behaviour under loading–unloading of semicrystalline polymers: application to a high density polyethylene, Int. J. Plast. 26 (2010) 329–347.
[36] D. Garcia-Gonzalez, R. Zaera, A. Arias, A hyperelastic-thermoviscoplastic constitutive model for semi-crystalline polymers: application to PEEK under dynamic loading conditions, Int. J. Plast. 88 (2017) 27–52.
[37] M.C. Boyce, E.M. Arruda, Constitutive models of rubber elasticity: a review, Rubber Chem. Technol. 73 (2000) 504–523.
[38] Y. Jia, K. Peng, X.L. Gong, Z. Zhang, Creep and recovery of polypropylene/carbon nanotube composites, Int. J. Plast. 27 (2011) 1239–1251.
[39] W. Zhang, A.L. Yarin, B. Pourdeyhimi, Cohesion energy of thermally-bonded polyethylene terephthalate nonwovens: experiments and theory, Polym. Test. 78 (2019) 105984.
[40] E. Demirci, M. Acar, B. Pourdeyhimi, V.V. Silberschmidt, Finite element modelling of thermally bonded bicomponent fibre nonwovens: tensile behaviour, Comput. Mater. Sci. 50 (4) (2011) 1286–1291.
[41] M.B. Rubin, An elastic-viscoplastic model exhibiting continuity of solid and fluid states, Int. J. Eng. Sci. 25 (1987) 1175–1191.
[42] M.B. Rubin, A time integration procedure for plastic deformation in elastic-viscoplastic metals, Z. Angew. Math. Phys. ZAMP 40 (1989) 846–871.
[43] M.B. Rubin, A.L. Yarin, On the relationship between phenomenological models for elastic-viscoplastic metals and polymeric liquids, J. Non-Newtonian Fluid Mech. 50 (1993) 79–88.
[44] M.B. Rubin, A.L. Yarin, On the relationship between phenomenological models for elastic-viscoplastic metals and polymeric liquids, J. Non-Newtonian Fluid Mech. 57 (1995), 321-321.
[45] A.L. Yarin, On instability of rapidly stretching metal jets produced by shaped charges, Int. J. Eng. Sci. 32 (1994) 847–862.
[46] B.E. Meserve, Fundamental Concepts of Algebra, Dover Publ., New York, 1982.